Contents list available at IJRED website

International Journal of Renewable Energy Development

Journal homepage: https://ijred.undip.ac.id

Research Article

Performance enhancement and emissions reduction in a diesel engine using oleander and croton biodiesel doped with graphene nanoparticles

Treza Wambui[1*], Meshack Hawi[2], Francis Njoka[3], Joseph Kamau[1]

[1]*Institute of Energy and Environmental Technology, Jomo Kenyatta University of Agriculture and Technology, P.O. Box 62000-00200, Nairobi, Kenya*

[2]*Department of Mechanical Engineering, Jomo Kenyatta University of Agriculture and Technology, P.O. Box 62000-00200, Nairobi, Kenya*

[3]*Department of Energy, Gas and Petroleum Engineering, Kenyatta University, P.O. Box 43844-00100, Nairobi, Kenya.*

Abstract. Biodiesel is considered a suitable substitute for petroleum diesel because it is renewable, environment-friendly, and has a low carbon footprint. However, its high density, high viscosity and low heating value prevents it from replacing petroleum diesel completely. This study investigates the performance and emission characteristics of a compression ignition engine operating on oleander and croton biodiesel doped with graphene nanoparticles. Five fuel samples are used, including diesel (D100), diesel - 80% blended with oleander and croton biodiesel - 20% (OCB20) and OCB20 dosed with graphene nanoparticles at mass fractions of 50 ppm (mg/L), 75 ppm (mg/L) and 100 ppm (mg/L), respectively. The chemical composition of biodiesel and graphene nanoparticles is analyzed using Fourier Transform Infrared (FTIR) spectroscopy while the morphology of the nanoparticles is analyzed using Scanning Electron Microscope (SEM). Engine tests reveal a significant improvement in brake thermal efficiency, especially at 75 ppm concentration which is 2.76% and 18.93% higher than diesel and OCB20, respectively, and a reduction in brake specific fuel consumption by 2.44% and 16.67% compared to diesel and OCB20, respectively. Carbon monoxide (CO) and unburnt hydrocarbon emissions (UHC) decreases for the 50 ppm sample, recording 8.58% and 21.65% reduction in CO and 52.2% and 50% in UHC compared to the diesel and OCB20, respectively. However, Oxides of Nitrogen (NOx) emissions increase. The results indicate that graphene nanoparticle-enhanced biodiesel can adequately substitute petroleum diesel, albeit with NOx reduction techniques.

Keywords: Biodiesel; Compression ignition engine; Emission; Nano additives; Engine Performance

Received: 14th January 2023; Revised: 17th April 2023; Accepted: 3rd May 2023; Available online: 15th May 2023

1. Introduction

The decline in fuel reserves, global industrialization and the increase in the number of vehicles on the road and the ever-growing world population have led to increased energy demand, especially for diesel engines, which are used widely in different sectors including power generation, automobile and industrial applications. Diesel engines are robust, more durable and have low fuel consumption compared to spark ignition engines, making them more attractive for most commercial applications. However, petroleum diesel is non-renewable and is associated with air pollution and global warming.

Due to the pressing energy concerns, health and environmental impacts, several researchers have investigated exhaust gas emission reduction techniques, including exhaust gas after-treatment, engine modification, combustion management and use of alternative fuels and fuel additives. Recent studies have shown that biodiesel fuel is a promising substitute for petroleum diesel since it is not only environment-friendly and renewable but also biodegradable (Yakasuwa *et al.,* 2013), sulphur free, oxygenated (Pattanaik *et al.,* 2017) and has a low carbon footprint (Hanaki *et al.,* 2018). Additionally, biodiesel is a good lubricant, thus reducing the tear and wear of the engine parts (Fazal *et al.*, 2013). Besides, its application does not require any engine modification.

Biodiesel is derived from animal fats and edible and non-edible oil feedstock such as croton, sunflower, oleander and castor oils through transesterification process. Oils from non-edible and drought-resistant feedstock are recommended to guard against food insecurity and reduce land competition with edible oil plants (Bhattacharyya, 2022). However, the performance of diesel engines run on biodiesel is a little inferior relative to fossil diesel owing to its high viscosity, high density and low heating value, which, if applied directly in compression ignition (CI) engines or in high proportion in diesel-biodiesel blends may lead to clogging of fuel lines, poor atomization and incomplete combustion as well as carbon deposits in the engine (Agarwal *et al.,* 2017).

Recent studies have shown that certain fuel additives in the form of nanoparticles (NPs) can enhance combustion while reducing emissions from diesel engines. Hence, many researchers have tested the application of different metal-based and non-metal NPs to enhance biodiesel combustion while reducing exhaust emissions (Devarajan *et al.,* 2018). High thermal conductivity coupled with exceptionally high surface area per unit volume possessed by NPs provides a wide dynamic surface for chemical reactions which improves

* Corresponding author
Email: treza.nganga@students.jkuat.ac.ke (T. Wambui)

https://doi.org/10.14710/ijred.2023.51785
ISSN: 2252-4940/© 2023.The Author(s). Published by CBIORE

combustion and reduces exhaust emissions (Mahdi and Nsofor, 2017). However, due to environmental and health concerns on the effect of metal-based NPs, non-metal NPs and specifically carbon-based NPs have gained prominence (Goswami *et al*., 2017) since they are devoid of any metal components, with a host of desirable chemical, physical, mechanical, and electrical characteristics. These additives possess attractive attributes such as excellent thermal conductivity and high surface area which makes them preferred candidates for biodiesel nano-additives (El-Seesy *et al*., 2018). Carbon-based NPs participate in exothermic reactions thus increasing the total released heat that eventually increases the calorific value of the base fuel (Sisim, *et al.,* 2020). Carbon-based nano-additives form a long-term stable dispersion in the base fuels with minimal particle agglomeration compared to metallic additives and thus do not necessarily require the use of a surfactant (Soudagar *et al.,* 2018). They are also combustible and therefore do not form any deposits in the CI engines hence reducing the chances of fuel system blockage, unlike metal-based NPs which may get deposited in engine components.

Graphene is one of the common organic additives considered by most researchers in recent decades owing to its remarkable properties which include high thermal conductivity of about 3000–5000 W/m/K (Sang *et al*., 2019), high electron mobility, high electrical conductivity and lightweight (Tony Pallone, 2018). Graphene is an allotrope of carbon, one atom thick with a 2D structure consisting of sp^2 bond. It has a high theoretical surface area of 2629 m^2/g (Igor Ivanov, 2019) the highest of all known materials which provides a wide dynamic surface for chemical reactions which improves combustion and reduces exhaust emissions (Mahdi & Nsofor, 2017). The small particle size coupled with the low density which is 2.0-2.25 g/cm^3 (Daud, Hamidi and Mamat 2022) makes it easily dissolvable in many hydrocarbon fuels without agglomerating, thereby forming stable colloids with the base fluid (Chehroudi, 2016). Graphene is preferred over other carbon-based nano additives such as graphene oxide and multi-wall carbon tubes (MWCT) because of its high calorific value (CV), superior engine performance and low emissions (EL-Seesy & Hassan, 2019). The doped GNPs are converted to CO_2 during combustion and taken up by plants during photosynthesis, unlike metal-based NPs which are emitted directly from the exhaust to the environment, causing environmental pollution. Because GNPs are fully oxidized in high-temperature combustion regions with nearly no additional residues other than the common combustion products, they can be regarded as fuel supplements that not only contribute towards energy density but also environment-friendly.

Debbarma *et al*., (2020) doped palm biodiesel-30% blended with diesel-70%, with GNPs at mass fractions of 50, 75 and 100 mg/L. They observed that the inclusion of GNPs resulted in 2.5% increase in BTE, 17% and 34% reduction in UHC and CO emissions, respectively, and 3.8% increase in NOx emission. Similarly El-Seesy *et al.,* (2018) mixed graphene nanoplatelets (GNPs) at 25, 50, 75 and 100 ppm on a mixture of 80% neat diesel and 20% Jatropha biodiesel. The results revealed a rise of 25% in BTE and a 20% reduction in BSFC relative to the neat biodiesel at 50-75 ppm dosing level. On the other hand, UHC, NOx and CO emissions decreased by 50%, 40%, and 60%, respectively, at 25–50 ppm concentration. Optimal engine performance and lowest emissions were realized at 50 ppm dosage. Razzaq *et al.,* (2021) experimented the effect of GONPs and DMC10 additives doped in palm biodiesel-30% and diesel-80% mixture at 40, 80 and 120 mg/L concentrations, on the performance and emissions of CI engine. They recorded a 22.80% increase in BTE, 3.65% and 5.05% reduction in NOx and BSFC, respectively, for the 40 ppm concentration and a 25% and 4.41% reduction in HC and CO respectively, for the un-doped fuel relative to all tested samples.

Mallikarjuna *et* al., (2022) demonstrated that the inclusion of GNPs to JME -20% and diesel - 80% (JME20), at concentrations of 25, 50, 75 and 100 ppm improves performance characteristics significantly, especially at 50 ppm concentration. NOx, CO, HC emissions and smoke are reduced significantly for the nano-enhanced blends compared to JME20. Bhagwat *et al.,* (2015) doped HOME with GNPs at 25 ppm and 50 ppm concentrations. They observed that doping the fuel with GNPs increased BTE and decreased UHC, CO, and NOx emissions relative to HOME. Optimal performance and minimum emission characteristics were achieved at 50 ppm concentration. Likewise, Nair *et al*., (2021) added GNPs to a mixture of 80% diesel and 20% Karanja (*Pongamia pinnata*) biodiesel at 25, 50 and 75 ppm. From the results obtained, the performance and emission characteristics of the nanoparticle-enhanced fuel were comparable to those of petroleum diesel. BTE for the nanoparticle-enhanced fuel increased significantly while BSFC, NOx and CO emissions reduced relative to Karanja biodiesel. The lowest HC emission was achieved at 75 ppm concentration except at zero load where diesel recorded the lowest. Sunilkumar *et al.,* (2017) conducted a study using WCOME doped with GNPs at 20, 40 and 60 mg/L concentrations and reported increased BTE, decreased BSFC and ignition delay, improved calorific value and lower HC and CO in comparison to the biodiesel, while NOx increased slightly.

In this work, Oleander and Croton oils are considered suitable feedstock for the synthesis of biodiesel since they are non-edible oils and therefore pose no threat to food security. In addition, the crops are drought resistant and can be grown on marginal land. Yellow Oleander seeds have a high oil content of more than 60% and a biodiesel yield of more than 80% and therefore can be harvested for large-scale biodiesel production (Yakasuwa, *et al*., 2013 and Basumatary & Deka., 2014). However, Yellow Oleander Methyl Ester (YOME) is not preferred for application in cold regions owing to its high cloud and pour points which are 12 ℃ and 2 ℃ respectively (Oseni & Obetta, 2012) which are higher compared to those of conventional diesel of 4 ℃ and -2 ℃, respectively (Osawa *et al.,* 2014). On the other hand, Croton megalocarpus oil (CMO) has remarkable cold flow properties of -1.5 ℃ - cloud point and -6.5 ℃- pour point, which has rendered it useful in cold regions (Osawa *et al.,* 2014). However, the low seed yield and low oil content render Croton feedstock unsustainable. From the foregoing, biodiesel from the two feedstocks complements each other.

From the review, it is evident that a blend of diesel and biodiesel doped with nanoparticles is a promising technique for enhancing engine performance and reducing exhaust emissions. However, there is scarce literature on the use of GNPs with biodiesel from certain feedstocks such as Oleander and Croton oil as fuel for diesel engines. The current work, therefore, seeks to establish the effects of adding GNPs to Oleander-Croton biodiesel and petroleum diesel blends on the performance and emission characteristics of a CI engine, as well as the most suitable GNPs concentrations for optimal engine performance.

2. Materials and Methods

2.1 Fuel Samples Preparation

2.1.1 Biodiesel and Nanoparticle Supplies

Petroleum diesel, Oleander and Croton biodiesels used in the current study were acquired commercially from local outlets

Table 1
Specifications of the nanoparticles

Description	Graphene nanoparticles
Manufacturer	Nano Shel-India
Carbon content	99.5%
Average particle size	2-4 nm thick, 5 µm wide
Thermal conductivity	3000 W/mK
Appearance	Black
Specific surface area	120-140 m^2/g
Morphology	Flaky
State	Amorphous powder
Average number of layers	3-6 layers

while graphene nanoparticles were sourced from NanoShel Company, India where it was synthesized using exfoliation method, the most preferred as it yields superior, defect-free, few-layered graphene with a larger surface area (Abbasi *et al.,* 2016). The specifications of GNPs are shown in Table 1.

2.1.2 Biodiesel blends preparation

Five fuel samples were used for the study including neat diesel denoted by D, diesel (80%) blended with 20% of Oleander and Croton biodiesel, denoted by OCB20 and OCB20 dosed with GNPs at mass fractions of 50 mg/L (50 ppm), 75 mg/L (75 ppm) and 100 mg/L (100 ppm) denoted by GNP50-OCB20, GNP75-OCB20 and GNP100-OCB20, respectively.

Oleander and Croton biodiesels were mixed in different proportions in a bid to establish the ratio that would yield a blend with the most desirable characteristics. From the results obtained, a mixture of 70% Oleander biodiesel and 30% Croton biodiesel yielded the lowest density and viscosity without compromising the calorific value. This blend was denoted by OCB. OCB-20% was blended with petroleum diesel-80% using a magnetic stirrer for about 20 min at 1000 rpm to form OCB20. The 20:80 biodiesel to diesel ratio was arrived at based on previous studies conducted by Sabapathy *et al.,* (2021) and Jalaludin, *et al.*, (2020). The physicochemical properties were evaluated according to ASTM D7467 and EN 14214 international standards.

2.1.3 Dispersion of GNPs to Oleander-Croton biodiesel/Diesel blend

GNPs were weighed accurately at a mass of 50 mg using a precision electronic balance and dispersed in a 2000 ml beaker containing 1 liter of OCB20 and mixed thoroughly using an ultrasonicator (Hielscher ultrasonic Model UP200S40) set at a frequency of 24 kHz, for 40 minutes, to prevent GNPs agglomeration in the OCB20 blend. The sample formed was denoted by GNP50-OCB20. The procedure was repeated for 75 ppm and 100 ppm to prepare GNP75-OCB20 and GNP100-OCB20 samples, respectively. The 50-100 ppm GNPs range was informed by a previous investigation by Debbarma *et al.,* (2020). The stability of the prepared samples was investigated using sedimentation and centrifugation techniques (Saxena et al., 2017), and was found stable and homogeneous for approximately 96 hours. Thereafter, the viscosity, density and calorific value of the sample fuels were measured using Redwood Viscometer model AN-823 manufactured by Nihon Abura Shikenki, Tokyo-Japan, hydrometer and adiabatic bomb calorimeter manufactured by Yoshida Seisakusho co, ltd Tokyo-Japan, respectively, using D- 445, D-240 and D-1298 ASTM testing methods respectively. The results were compared with those of EN14214 and ASTM 7467 international standards for conformity. The prepared samples were tested on a stationary single-cylinder four-stroke multi-fuel CI engine and

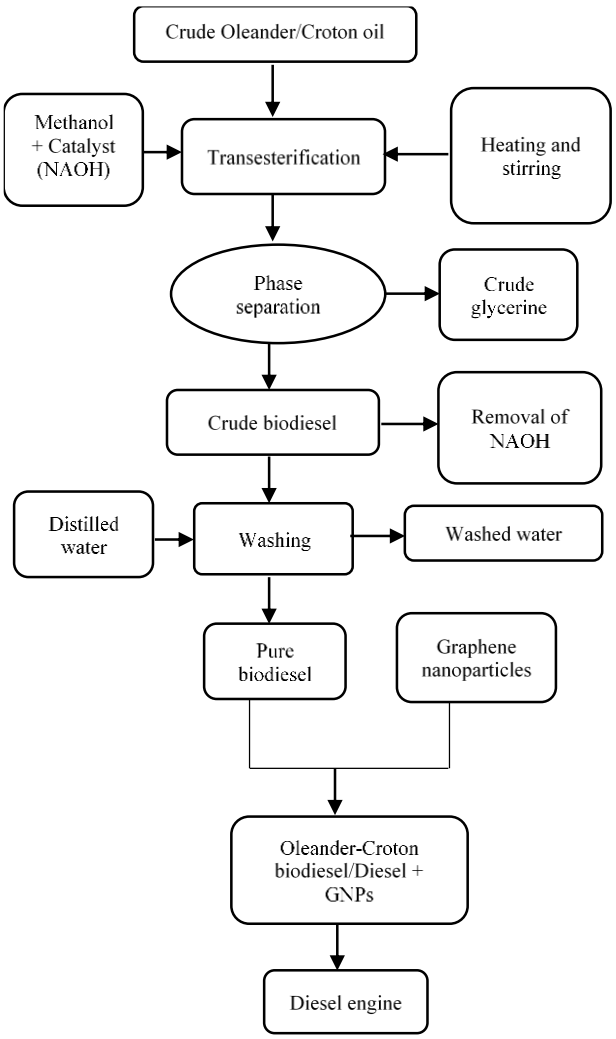

Fig. 1 Schematic of biodiesel production and fuel blends preparation process

performance parameters, including, BSFC and BTE as well as NOx, UHC and CO emissions investigated. Fig.1 illustrates a schematic of the biodiesel production process and tests in the engine.

2.2 Determination of engine performance and emission characteristics.

2.2.1 Engine experimental setup

The experimental set-up consists of a four-stroke, single-cylinder compression ignition engine integrated with an eddy current dynamometer for loading and controlling the speed of the engine. The setup comprises a separate panel box that consists of a fuel tank, air box, fuel gauge unit, and fuel and air gauge transmitters. Measurement of calorimeter water and the engine cooling water flow rates is accomplished with the aid of a rotameter. A proximity switch connected to the engine shaft is used to determine the instantaneous position of the piston TDC while the crank angle is determined using a crank encoder with a resolution of 1°, 5500 RPM with a TDC pulse. Piezoelectric pressure sensor model 601A was employed for measuring instantaneous in-cylinder pressure while the temperature of exhaust gases and cooling water was determined using K-type thermocouples. Signals from the pressure sensor, air flow sensor, speed sensor, load sensor, crank angle sensor and fuel flow sensor are transmitted to the Data Acquisition Device model NI USB-6210, 16-bit, 250kS/s

Table 2
Diesel Engine and Exhaust Gas Analyzer Specifications

Engine parameters	Specifications
Engine model	Kirloskar, 1-cylinder, 4-stroke, diesel engine
Bore	87.5 mm
Compression ratio range	12:1–18:1
Stroke	110 mm
Cooling system	Water cooled
Rated power	3.5 kW@1500 rpm
Ignition system	Compression ignition

Gas analyzer specifications			
Gas	Measuring range	Resolution	Accuracy
CO	0 – 5000 ppm	1 ppm	±5% of reading or ±10 ppm
CO_2	0 – 20% by vol.	0.1% by vol.	0.5% of reading
UHC	0–40000 ppm	1 ppm	±0.3% of reading
NOx	0 – 500 ppm	1 ppm	±5% of reading or ±5 ppm
O_2	0 – 25% by vol.	0.01% by vol.	±0.3%

and controlled by ICEngineSoft 9.0 software, developed by Apex Innovations Pvt Ltd-India. A Testo Eassy Emission analyser 350 (software 2.9) and calorimeter are attached to the engine's exhaust for the measurement of emissions and estimation of the heat carried away by exhaust gases, respectively. Table 2 shows the specifications of the engine and emissions analyzer.

2.2.2 Experimental procedures

Engine performance tests were conducted on a stationary single-cylinder four-stroke CI engine with a compression ratio set at 17:1 and loads of 0%, 25%, 50%, 75% and 100% chosen based on previous experiments conducted on the same engine. The fuel tank was filled with diesel and ran for approximately 10 minutes to attain steady-state conditions, after which measurements were recorded at zero set load at a constant speed of 1250 rpm.

Measurement of CO, UHC and NOx emissions was accomplished using an emissions analyzer while engine performance characteristics (BTE and BSFC) were obtained using ICEngineSoft 9.0 software. Ten consecutive emission values for every fuel sample were recorded and averaged for accuracy. After taking measurements at no load, the engine was then loaded to 25%, 50%, 75%, and finally to 100% loads, each

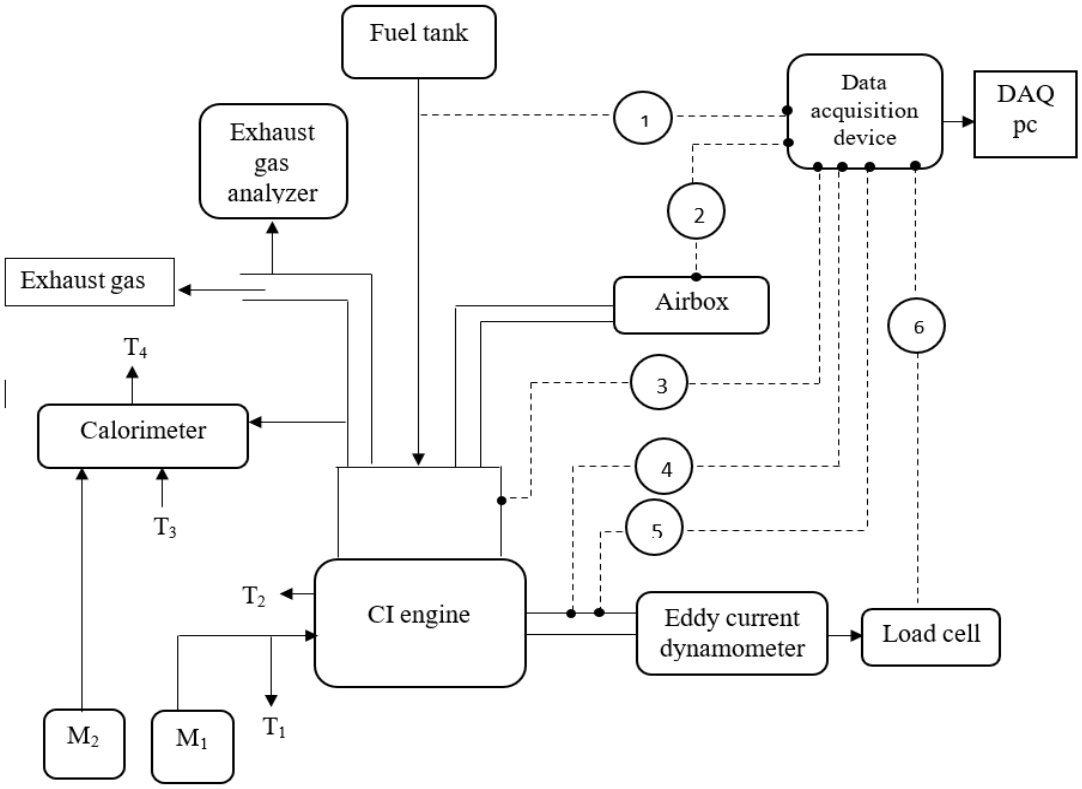

1. Fuel flow sensor
2. Air flow sensor
3. Pressure sensor
4. Speed sensor
5. Crank angle sensor
6. Load sensor

$\mathbf{T_1}$ Temperature of cooling water to the engine
$\mathbf{T_2}$ Temperature of cooling water from the engine
$\mathbf{T_3}$ Temperature of cooling water to calorimeter
$\mathbf{T_4}$ Temperature of cooling water to calorimeter
$\mathbf{M_1}$ Engine cooling water flow meter
$\mathbf{M_2}$ Calorimeter cooling water flow meter

Fig. 2 Schematic of the engine setup

load at a time, for every sample after which emissions and engine performance characteristics were recorded.

The neat diesel was then drained and the tank was filled with the OCB20 blend and other samples, each at a time and the process repeated. For every load, the engine parameters were recorded and transmitted to the Data Acquisition Device for analysis and subsequent conversion from analogue to digital format, then displayed in real-time on the DAQ PC, in both graphical & numerical formats. Eventually, the engine was run on neat diesel to flash out any residuals of the sample fuel from the injection system. The schematic of the engine setup is illustrated in Fig. 2.

2.3 Experimental uncertainty

Uncertainty analysis is essential for quantifying the uncertainty in the measured data. It aids in the determination of the repeatability and precision of the experimental results. The sources of error include instruments used for the measurement, human errors, or environmental conditions. The size of the error was minimized by considering the mean of three readings under a constant operating condition, which showed a spread about the mean (Soudagar, Nik-Ghazali, *et al.,* 2020). The current study employed a student's t-test for the error analysis since the sample size was small.

The mean ($\bar{x}$), Variance ($\sigma^{2)}$ and standard deviation (σ) for the sample size (n) were obtained using equations (1), (2) and (3) respectively while the error was calculated using equation (4) (Jeyaseelan & Chako, 2020).

$$\bar{x}=\frac{1}{n}\sum_{i=1}^{N} x_i \quad (1)$$

$$\sigma^2 = \frac{1}{n-1}\sum_{i=1}^{N}(x_i-\bar{x})^2 \quad (2)$$

$$\sigma = \left(\frac{1}{n-1}\sum_{i=1}^{N}(x_i-\bar{x})^2\right)^{\frac{1}{2}} \quad (3)$$

$$Error, \Delta = \frac{t\times\sigma}{n} \quad (4)$$

Where t is the value obtained from student's t-table with a degree of freedom of n -1 at 95% confidence level (or 0.05 significance level). The error margin for BTE and BSFC for the 5 fuel samples tested is as shown in Table 3 while that of CO, HC and NO_X is ± 5%, ± 0.3% and ± 5% respectively, provided by the manufacturer. From Table 3, it can be seen that the values for the mean for the three runs in each treatment are less than 0.05 implying there is no significant difference between the values obtained for each run for the treatment in consideration. Table 4 shows the measurement range and accuracy of instruments used in the study.

Table 3
Error margin for BTE and BSFC at 95% confidence level and degree of freedom of n-1.

Test fuels	Parameter measured	
	BTE	BSFC
D100	± 0.024	± 0.0024
OCB20	± 0.051	± 0.0014
GNP50-OCB20	± 0.051	± 0.0024
GNP75-OCB20	± 0.030	± 0.0024
GNP100-OCB20	± 0.033	± 0.0014

3. Results and Discussions

3.1 Characterization of biodiesel and graphene nanoparticles

The chemical composition of the biodiesel and GNPs was ascertained through Fourier-Transform Infrared (FT-IR) analysis which identified the presence of various functional groups in the biodiesels and graphene nanoparticles. The experiment was conducted using Bruker Alpha FTIR Spectrometer Model Vertex 70, at a wavelength range of 4000-500 cm^{-1}. The surface and morphological characterization of GNPs, on the other hand, was investigated using Scanning Electron Microscope (JEOL JCM 7000).

3.1.1 FTIR analysis for biodiesels and petroleum diesel

FTIR analysis was conducted on Oleander and Croton biodiesel, petroleum diesel and OCB20, and the spectrum for the fuels compared, as illustrated in Fig.3. The appearance of strong absorption peaks at approximately 1750 cm^{-1} for Oleander biodiesel, Croton biodiesel and OCB20 spectra represents C=O stretching vibrations which indicates the presence of an ester carbonyl bond (Nandiyanto *et al.,* 2019), while those at approximately 1165 cm^{-1} represents C-O stretching vibrations. The appearance of these two sets of peaks confirms the presence of an ester group in the biodiesel (Yohannan *et al.,* 2011). These peaks were absent in the diesel fuel because the latter as no oxygen content nor the ester group in its structure (Ruhul *et al.,* 2015). The absorbance peaks observed at approximately 2860 cm^{-1} and 2970 cm^{-1} for all the

Table 4
Accuracy of measuring instruments

S/no.	Instrument	Measuring range	Accuracy (±)
1	Dynamometer	560 Nm	1.68 Nm
2	Air flow meter	160 m^3/h	1m^3/h
3	Pressure sensor	0-250 bar	1.118%
4	Thermocouples	0-1300 K	1°C
5	Load indicator	250-5000 W	10 W
6	Crank angle encoder, degree	0–720	0.5
7	Speed sensor, rpm	0–10,000	5 rpm
8	Fuel burette, cc	153	0.2
9	Torque indicator, Nm	0–200	±1% of reading

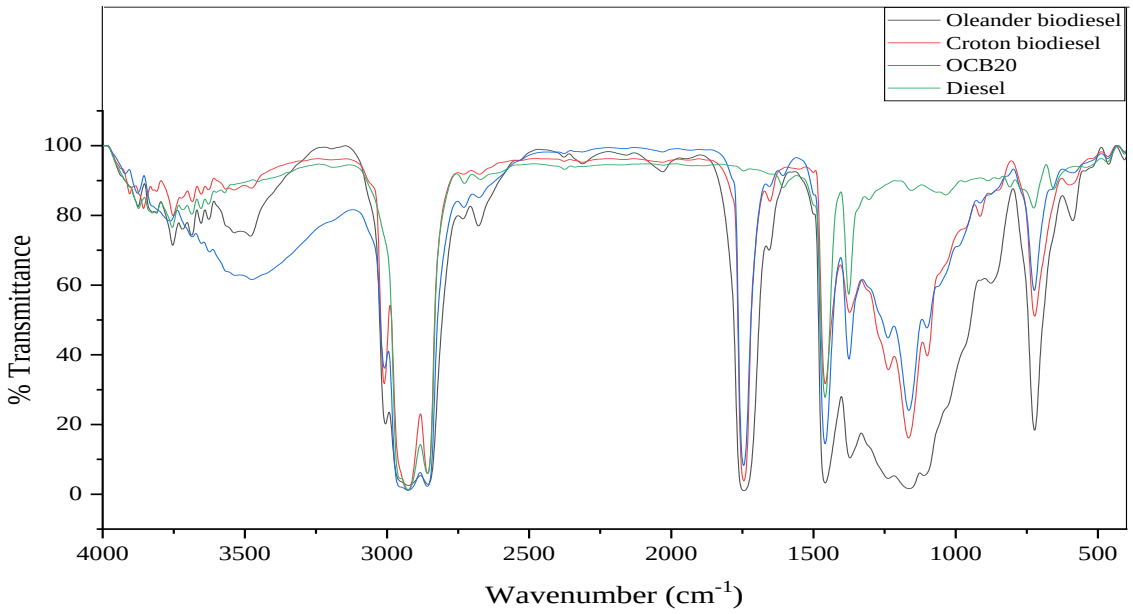

Fig. 3 FTIR spectrum of Oleander and Croton biodiesel, OCB20 and Petroleum diesel.

fuel samples revealed the existence of symmetric and antisymmetric stretching vibrations of the C-H bond in CH_3 and CH_2 groups respectively, while those at approximately 1480 cm^{-1} and 723 cm^{-1} represented Methylene C-H bend, both of which belong to the alkanes family. The existence of C-H bonds (hydrocarbon) is an indicator that the molecules under investigation have the potential to be used as fuels. The percentage transmittance for the OCB20 was lower than that of diesel which pointed to the introduction of more bonds in the sample that absorbed the energy at that particular wavenumber. Qasim, Ansari and Hussain (2017) and Coronado *et al.*, (2017) reported similar FTIR spectra results from a mixture of waste Canola and waste transformer oils blended with petroleum diesel and waste vegetable oil blended with petroleum diesel at different concentrations, respectively.

3.1.2 FTIR analysis for GNPs

The chemical structure of GNPs was ascertained using the FTIR spectrum as depicted in Fig. 4. The analysis focused on the functional group region (1400 cm^{-1}- 4000 cm^{-1}) as it is the most reliable region regarding spectrum interpretation compared to the fingerprint region (1400-500), (Wade, Jr., 2003). The sharp narrow peak observed at 1399.86 cm^{-1} was attributed to the C–C stretch (in ring) vibrations in the aromatic ring, while the peak at 1597.10 cm^{-1} indicates the presence of C=C-C aromatic ring stretch vibration (Nandiyanto *et al.,* 2019) which is a dominant covalent bond in the graphene structure (Kamel *et al.,* 2020). The peak at 3131.87 cm^{-1} denoted the existence of an aromatic C-H stretching mode (Nandiyanto *et al.,* 2019). Both 1597.10 cm^{-1} and 3131.87 cm^{-1} peaks belong to the arly functional group to which graphene is a member (Ujjain et al., 2019).

3.1.3 SEM analysis for GNPs

The structure, shape and form of the crystals is very important in nanocomposites as it helps to evaluate the mechanical and chemical properties of the nanoparticles under investigation (Sivasankaran *et al.*, 2011). Fig. 5 (a) and (b) shows SEM images of GNPs at x500 and x2000 magnification, respectively. The

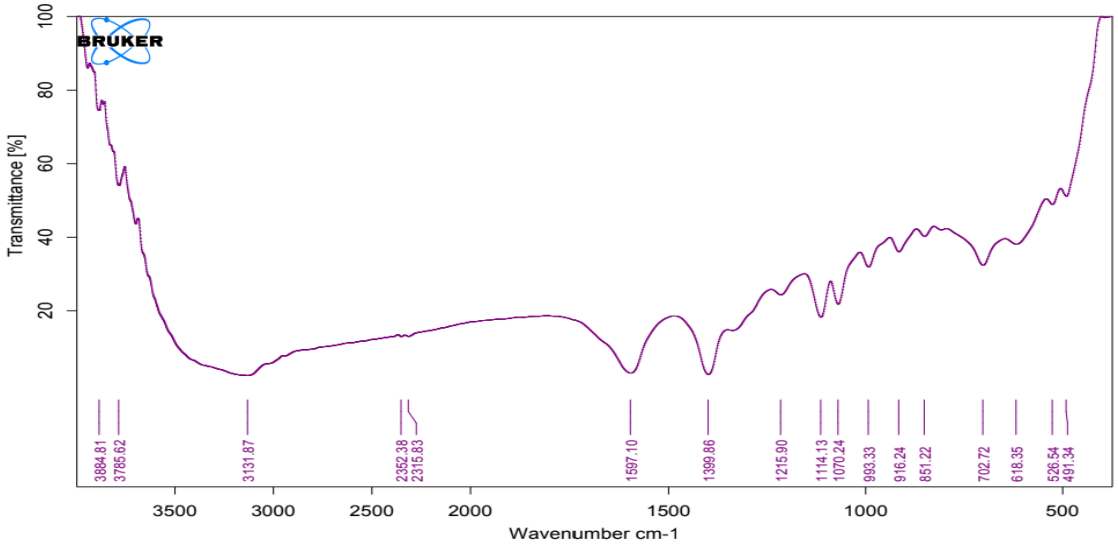

Fig. 4 FTIR spectrum of GNPs

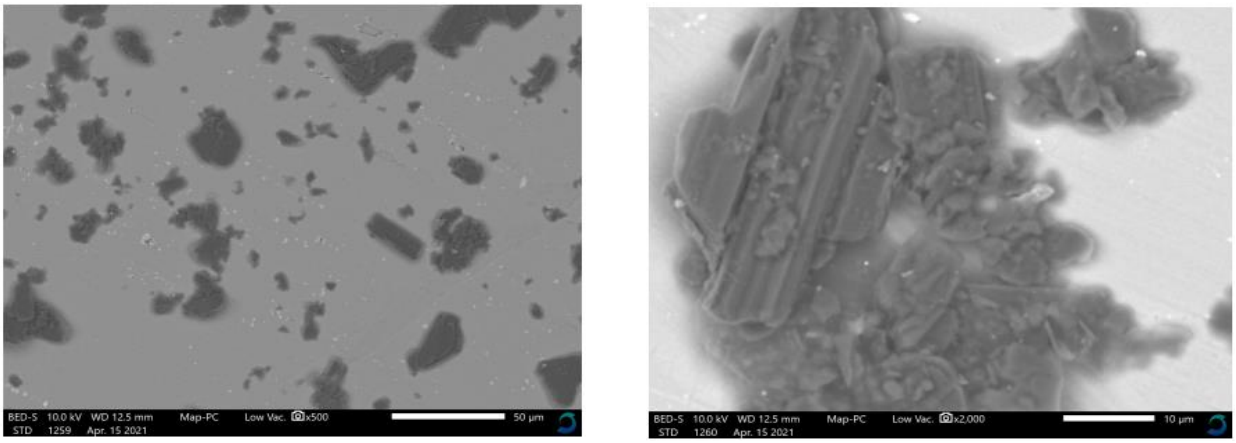

Fig. 5 SEM images of GNPs at (a) x500 magnification and (b) x2000 magnification

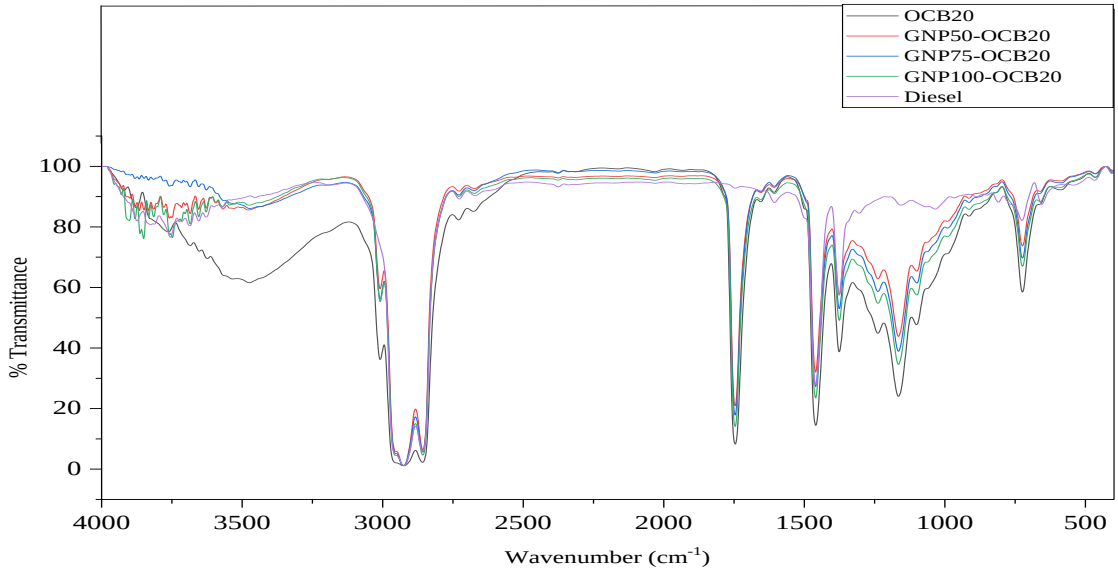

Fig. 6 FTIR spectra for petroleum diesel, OCB20 and OCB20 enhanced with GNPs at 50 ppm, 75 ppm and 100 ppm

images show that the nanoparticles are spherical, with a flaky surface of approximately 5.0 µm wide, amorphous (Antidormi *et al.,* 2022), and are clustered. A closer look at Fig. 5 (b) reveals the corrugated structure of graphene (Deng & Berry, 2016), which contributes significantly to its high surface area leading to enhanced heat transfer (Begag *et al.,* 2021).

3.1.4 Comparison of FTIR spectra for OCB20, Petroleum diesel and GNPs-enhanced fuels.

The FTIR spectra for petroleum diesel, OCB20 and OCB20 enhanced with GNPs at 50 ppm, 75 ppm and 100 ppm concentrations were analysed and presented as shown in Fig. 6. The peak at wave number 3500 cm^{-1} was strong and broad for the OCB20 sample compared to that of the petroleum diesel and nano-enhanced samples, with that for petroleum diesel being the weakest. This was attributed to the existence of hydroxyl functional group O-H which is absent in graphene (Kamel *et al.,* 2020) and petroleum diesel (Masera & Hossain, 2017). OCB20 recorded the lowest intensity peaks (percentage transmittance) especially at approximately 1730 cm^{-1}, 1480 cm^{-1}, 1165 cm^{-1} and 725 cm^{-1} compared to those of petroleum diesel and GNP-enhanced samples. The reason could have been that; C=C and C-C bonds in GNPs have a higher peak intensity of approximately 10% compared to the C-O, C=O and C-H bonds in biodiesel which is less than 5%, as can be seen in the GNPs IFTR spectrum (Fig. 4). The increase in peak intensities in the FTIR spectra points to the inclusion of GNPs in the biodiesel blend.

3.2 Fuel physicochemical properties

The physicochemical properties of D100, OCB20, GNP50OCB20, GNP75OCB20 and GNP100OCB20 fuels were measured according to the prescribed testing methods and the results were compared with those of EN14214 standards for conformity. Table 5 presents the physicochemical properties of the test fuels.

3.3 Engine performance characteristics

Engine performance tests were done on a stationary CI engine. BTE and BSFC for all fuel samples were analysed and discussed in the following sub-sections.

Table 5
Properties of the test fuels

Fuel Property	Testing Method	Diesel	OCB20	GNP50OCB20	GNP75OCB20	GNP100OCB20	EN14142
Density @15 °C, g/cm^3	ASTM D-1298	0.827	0.850	0.852	0.854	0.856	0.860-0.900
Kinematic viscosity @40 °C, mm^2/s	ASTM D-445	2.02	3.60	8.638	8.756	9.757	3.5 - 5.0
Calorific value, kJ/kg	ASTM D-240	42,462	41,759	42,657	41,427	41,167	-

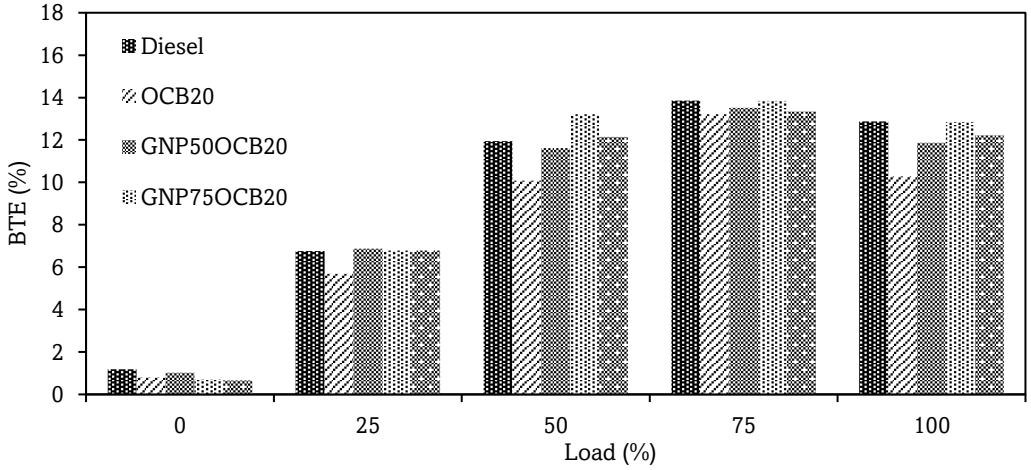

Fig. 7 Change of brake thermal efficiency with load

3.3.1 Brake thermal efficiency (BTE)

Brake Thermal Efficiency (BTE) is the ratio of the power input to the engine to the power output from the engine shaft. It specifies the ability of the engine to convert chemical energy in the fuel to mechanical power. Fig. 7 illustrates the variation of BTE with load for D100, OCB20 and fuel blends with GNPs. From the figure, BTE for all samples increased with the load up to 75% and then decreased marginally at full load. The BTE observed for OCB20 was 13.6% lower than that of D100 while that for GNP50OCB20 was on average 3.48% lower compared to that of D100 and 11.72% higher than that of OCB20 especially at higher loads. GNP75OCB20 recorded the highest BTE overall, which was 2.76% and 18.93% higher than that of D100 and OCB20, respectively, while OCB20 recorded the lowest. BTE for GNP100OCB20 was 2.09% lower than that of D100 and 13.33% higher than that of OCB20.

The increase in BTE with load was probably caused by the increase in the fuel supply, hence the availability of more fuel for combustion, while the decrease at full load could have been occasioned by the increased fuel-to-air ratio which reduced the combustion efficiency. This trend agrees with that reported by Debbarma *et al.,* (2020) and Sunilkumar *et al.,* (2017). On the other hand, the reduction in BTE for OCB20 compared to D100 was traced to the reduced CV, increased viscosity and density of the fuel blend relative to D100, while the reduction in relation to the doped fuels was ascribed to the absence of GNPs which resulted in reduced fuel atomization and consequently lowered combustion efficiency. Bhagwat *et al.,* (2015) observed similar results for HOME with GNPs. The reduction of BTE for the GNP50OCB20 sample relative to D100, more so at higher loads was probably occasioned by the presence of biodiesel and GNPs in the fuel blend which increased the density and viscosity of the fuel. On the other hand, its increase compared to OCB20 was possibly due to the increased CV and the inclusion of GNPs which enhanced chemical reactivity and thermal conductivity. The highest BTE recorded for the GNP75OCB20 fuel may have been occasioned by the increase in GNPs concentration whose

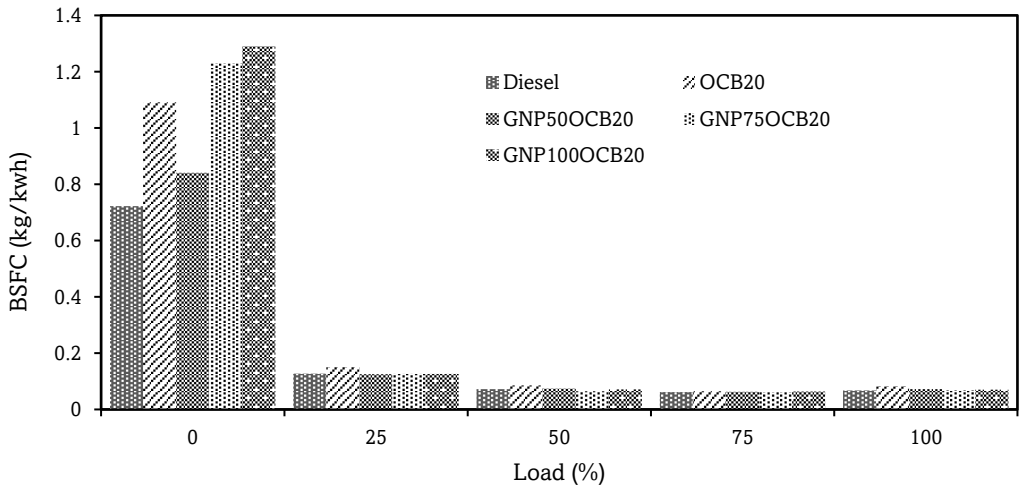

Fig. 8 Change of BSFC with load

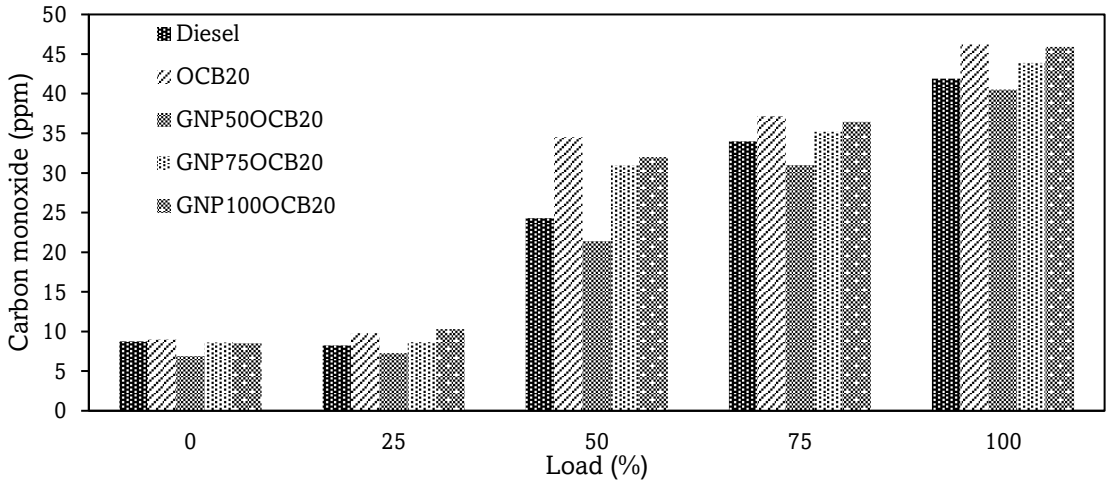

Fig. 9 Change of carbon monoxide with load

catalytic activity improved chemical reactivity significantly. Besides, the presence of GNPs improved thermal conductivity and oxidation of carbon hence ensuring efficient combustion (El-Seesy, *et al.,* 2018). This observation is in line with the findings of Mallikarjuna *et al.,* (2022) for Jatropha biodiesel blend enhanced with GNPs. The inferior BTE for GNP100OCB20 relative to D100 was attributed to increased concentration of GNPs which increased the density and viscosity of the nanoparticle-enhanced fuel, that not only caused poor fuel atomization during combustion but also may have resulted in degradation of the thermal performance of the Nanofluid, while the increase relative to OCB20 was probably due to increased catalytic activity and high energy content of GNPs. These results closely agree with those obtained by El-Seesy *et al.,* (2018) and Debbarma *et al.,* (2020) for GNPs in Jatropha biodiesel and GNPs in Palm biodiesel, respectively.

3.3.2 Brake Specific Fuel Consumption (BSFC)

BSFC is the specific amount of fuel consumed against the brake power generated. Fig. 8 illustrates the variation of BSFC with engine load for D100, OCB20 and blends with GNPs. From the figure, BSFC is highest at no load condition. It decreases as the load increases up to 75%, then increases marginally at full load. The lowest BSFC was recorded at 75% load for all samples. The BSFC for OCB20 was the highest, which was 17.07% higher than that of D100, while GNP75OCB20 recorded the lowest on average, which was 2.44% and 16.67% lower than that of D100 and OCB20, respectively. GNP100OCB20 on the other hand, recorded a BSFC 1.22% higher than that of D100 and 13.54% lower than that of OCB20.

The BSFC was highest at no load condition owing to the low temperature in the cylinder which consequently resulted in low fuel conversion efficiency. Nair *et al.,* (2021) noted a similar trend for Karanja (*Pongamia pinnata*) biodiesel- diesel mixture with GNPs. The reduction in BSFC as the load increased followed by the marginal increment at full load was possibly because the engine operates with a lean mixture at lower loads compared to full load conditions. This observation agreed with that of Nair *et al.,* (2021). The high BSFC for OCB20 relative to all the other fuels could have been occasioned by the high density, high viscosity and low CV of the blend which resulted in poor fuel atomization and less efficient combustion compared to other fuels, while the reduction in BSFC for GNP75OCB20 was attributed to the increase in the GNPs concentration that resulted in enhanced thermal conductivity and chemical reactivity. The high BSFC recorded for the GNP100OCB20 sample compared to D100 was ascribed to the high viscosity, CV and density of the fuel compared to D100, while the reduction compared to that of OCB20 could have resulted from the catalytic effect of the GNPs. These results agreed with those of Mallikarjuna *et al.,* (2022), from a mixture of Jatropha biodiesel blend with GNPs.

3.4 Emission Characteristics

The effect of GNPs on CI engine exhaust gas emissions (CO, UHC, NOx) at different engine load conditions was analysed and the results were discussed in the following sections.

3.4.1 Carbon Monoxide (CO)

CO is a toxic hydrocarbon combustion product in CI engines formed as a result of incomplete combustion occasioned by insufficient supply of O_2 molecules. Deviation of CO with load for D100, OCB20 and OCB20-GNPs blended fuels is illustrated in Fig. 9. CO emission increases slightly at 25% load relative to no load but increases significantly at full load for all fuel samples. CO emission for OCB20 was the highest, at 16.69% higher than that of D100 while the lowest CO emission was achieved with GNP50OCB20, which was 8.58%, 21.65%, 15.87%, and 19.56% lower relative to D100, OCB20, GNP75OCB20 and GNP100OCB20, respectively. On the other hand, CO emissions for GNP75OCB20 and GNP100OCB20 samples were higher than that of D100. However, CO emission for GNP75OCB20 was 6.88% lower than that of OCB20. The marginal increase of CO at no load and low load was attributed to the low fuel supply while the subsequent increase at higher loads was possibly due to the rich fuel mixture hence more emission. The high emissions for OCB20 relative to D100 and GNPs-enhanced fuels may have been occasioned by the low CV, high viscosity and high density compared to D100, and the absence of GNPs, respectively, which resulted in poor air-fuel mixing that led to incomplete combustion. The findings agreed closely with those of Sunilkumar *et al.,* (2017) for WCOME blend with GNPs. The low CO emission achieved with GNP50OCB20 was ascribed to improved combustion occasioned by the addition of GNPs to the fuel, which enhanced chemical reactivity and thermal conductivity leading to better conversion of CO to CO_2. The high CO emission recorded for GNP75OCB20 and GNP100OCB20 samples compared to D100 may have been caused by the increased GNPs concentration in the sample fuels which increased viscosity and density of the mixture relative to D100 leading to poor fuel atomization and hence inferior combustion of the fuel. The density and viscosity of the fuel

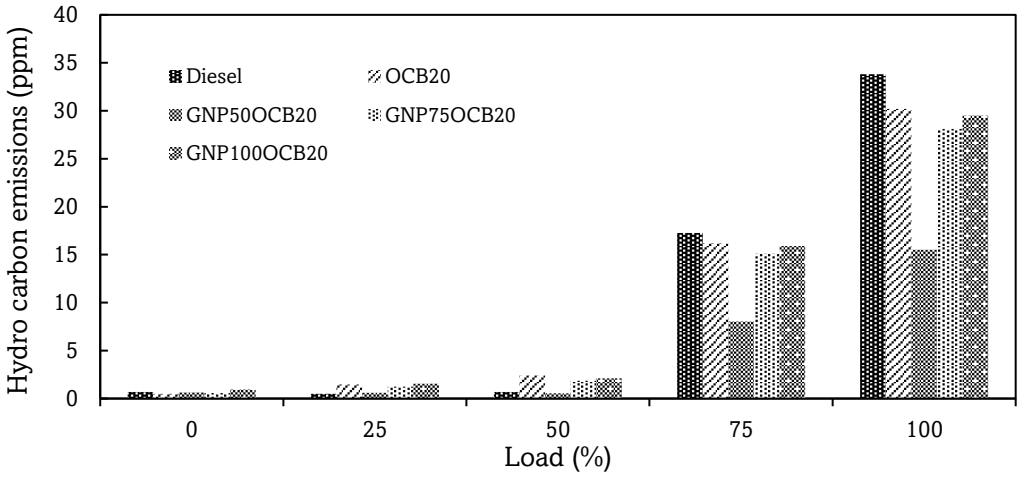

Fig. 10 Change of unburned hydrocarbon emission with load

increased with the increase in GNPs dosage, hence higher CO emission for GNP100OCB20 compared to other fuel samples with NPs. These findings are similar to those of Razzaq *et al.,* (2021) for Palm biodiesel blends with GONPs and DMCs NPs.

3.4.2 Unburned hydrocarbon (UHC)

Change in HC emission with the load for D100, OCB20 and OCB20-GNPs blended fuels is presented in Fig. 10. At lower loads, HC emission was low but increased at higher loads. HC emission for OCB20 increased with reference to D100 at lower loads and decreased as the load increased, allowing the UHC emission levels of D100 to be the highest at higher loads. The lowest emission level was achieved for the GNPs-enhanced fuels, with GNP50OCB20 recording the lowest which was 52.2% and 50% relative to D100 and OCB20, respectively. However, the UHC emission increased with an increase in GNPs dosage, resulting in emissions of GNP75OCB20 and GNP100OCB20 doubling relative to those of GNP50OCB20 samples. A drop of 11.52% and 5.57% for GNP75OCB20 and 7.59% and 1.38% for GNP100OCB20 compared to D100 and OCB20, respectively, was observed.

The low UHC emission at low loads and the subsequent increase as load increased was traced to the fact that at no load and low loads, minimal fuel is supplied, hence a lean mixture with improved combustion efficiency. At high loads, the fuel supply is increased to service the load demand, which in turn increases the fuel-air ratio which results in higher UHC emission. This agrees with the findings of Gad *et al.*, (2018). The higher UHC emission for OCB20 compared to D100 at lower loads was probably due to lower CV and high density and viscosity compared to that of D100 which resulted in inferior fuel atomization that led to incomplete combustion. On the other hand, the high UHC for diesel, specifically at higher loads, was attributed to less O_2 available for oxidation of the fuel compared to biodiesel with additional Oxygen from its molecular structure. The findings agree with those of Debbarma *et al.,* (2020).

GNPs-enhanced fuels recorded the lowest UHC emission with GNP50OCB20 taking the lead. This was ascribed to the high catalytic activity of GNPs coupled with the high O_2 content in the biodiesel which may have improved the combustion of hydrocarbons to products of complete combustion. On the other hand, the increase of emission for GNP75OCB20 and GNP100OCB20 relative to GNP50OCB20 may have been due to the increase in viscosity, density and reduction in the CV of GNP75OCB20 and GNP100OCB20 resulting from the higher quantity of GNPs in the fuel blends.

3.4.3 Oxides of Nitrogen (NOx)

NOx is a toxic gas emitted by CI engines as a result of O_2 and nitrogen interacting at high temperatures. Its formation is directly proportional to the combustion flame temperature inside the cylinder. Deviation of NOx with load for D100, OCB20 and GNPs-enhanced fuel samples is demonstrated in

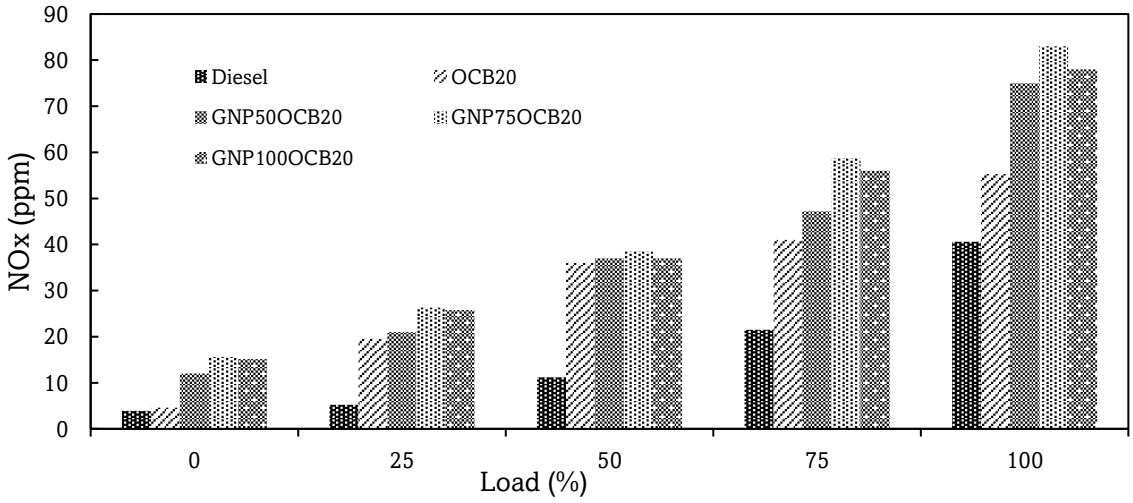

Fig. 11 Change of oxides of Nitrogen emission with load

Fig. 11. NOx emission increased alongside the load for all samples tested. NOx emitted for nanoparticle-enhanced fuel samples was higher than that of D100 and OCB20, with GNP75OCB20 recording the highest. D100 recorded the lowest. The increase in NOx emission alongside the load for all fuel samples tested was ascribed to the fact that at high load, more fuel is combusted which in turn releases more heat. This results in increased average gas temperature which oxidizes the nitrogen in the air leading to NOx formation (Semakula &Inambao, 2018). This trend is similar to that observed by Bhagwat *et al.,* (2015). The low NOx emissions recorded for D100 were possibly due to less oxygen to react with nitrogen to form NOx compared to biodiesel, since biodiesel has extra oxygen in its chemical structure (Pham, 2015). Additionally, the availability of more oxygen facilitated the combustion of fuel, which increased the temperature inside the chamber. This high temperature aided the reaction of oxygen with atmospheric nitrogen thereby forming NOx. Mallikarjuna *et al.*, (2022) and Debbarma *et al.,* (2020) reported a similar trend. On the other hand, the high NOx emission for GNPs-enhanced fuels compared to that of D100 and OCB20 was ascribed to high combustion temperatures resulting from enhanced combustion due to the rich air-fuel mixture occasioned by the addition of GNPs. This closely agrees with the findings of Mallikarjuna *et al.*, (2022). GNP75OCB20 produced the highest NOx emission possibly occasioned by the high gas temperature in the combustion chamber for that concentration which led to the oxidation of some of the nitrogen in the air to NOx, hence the increase in NOx emission.

4. Conclusions

Performance and emissions of a compression ignition engine fueled with Oleander-Croton biodiesel-diesel blend (OCB20) and OCB20 with GNPs at dosing levels of 50 ppm (50 mg/L), 75 ppm (mg/L) and 100 ppm (mg/L) were investigated. From the results obtained, it can be concluded that adding GNPs to the fuel blend improves brake thermal efficiency and reduces specific fuel consumption significantly, especially at 75% loading condition, with the optimum performance being achieved at 75 ppm dosing level. The presence of GNPs improves emission characteristics by lowering carbon monoxide and hydrocarbon emissions significantly at 50 ppm GNPs dosage compared to biodiesel-diesel mixture and neat diesel. However, it results in an increase in NOx emission compared to both biodiesel-diesel blend and petroleum diesel. From the results, it can be concluded that Oleander-Croton biodiesel-diesel blend mixed with GNPs can be used as a substitute fuel for diesel engines for the improvement of engine performance and reduction of UHC and CO emissions. However, since this is achieved with a slight increase in NOx emission, suitable NOx reduction techniques can be considered.

Acknowledgements

This study was partly funded by Japan International Corporation Agency (JICA) through AFRICA-ai-JAPAN Project and partly by the Pan African University Institute for Basic Sciences, Technology and Innovation (PAUSTI). The authors would also like to acknowledge Jomo Kenyatta University of Agriculture and Technology (JKUAT) for the provision of laboratory facilities.

Authors Declaration

The authors declare no known conflict of interest as far as the publication of this article is concerned.

References

Abbasi, E., Akbarzadeh, A., Kouhi, M., & Milani, M. (2016). Graphene: Synthesis, bio-applications, and properties. *Artificial Cells, Nanomedicine and Biotechnology*, *44*(1), 150–156. https://doi.org/10.3109/21691401.2014.927880

Agarwal, A. K., Gupta, J. G., & Dhar, A. (2017). Potential and challenges for large-scale application of biodiesel in automotive sector. In *Progress in Energy and Combustion Science,* 61 (July) 113-149; https://doi.org/10.1016/j.pecs.2017.03.002

Antidormi, A., Colombo, L., & Roche, S. (2022). Emerging properties of non-crystalline phases of graphene and boron nitride based materials. In *Nano Materials Science,* 4 (1), 10-17; https://doi.org/10.1016/j.nanoms.2021.03.003

Basumatary, S., & Deka, D. C. (2014). Transesterification of yellow oleander (Thevetia peruviana) seed oil to fatty acid methyl esters (biodiesel) using a heterogeneous catalyst derived from rhizome of Musa balbisiana colla. *International Journal of ChemTech Research*, *6*, 2377–2384. https://sphinxsai.com/2014/vol6pt4/3/(2377-2384)Jul-Aug14.pdf

Begag, A., Saim, R., Abboudi, S., & Öztop, H. F. (2021). Effect of internal and external corrugated surfaces on the characteristics of heat transfer and pressure drop in a concentric tube heat exchanger. In *International Journal of Thermal Sciences* 165 (July); https://doi.org/10.1016/j.ijthermalsci.2021.106930

Bhagwat, V. A., Pawar, C., & Banapurmath, N. R. (2015). Graphene Nanoparticle - Biodiesel Blended Diesel Engine. *International Journal of Engineering Research & Technology (IJERT)*, *4*(02), 75–78. https://www.ijert.org/research/graphene-nanoparticle-biodiesel-blended-diesel-engine-IJERTV4IS020094.pdf

Bhattacharyya, S. (2022). Transesterification of Yellow Oleander seed oil, its utilization as biodiesel and performance evaluation. In *Heliyon*, 8(4); https://doi.org/10.1016/j.heliyon.2022.e09250

Chehroudi, B. (2016). Applications of Graphene in Fuel Propellant Combustion Chehroudi 26 Applications of Graphene in Fuel/Propellant Combustion. *Graphene Science Handbook*, *May*. www.advtechconsultants.com

Coronado, M. A., Montero, G., García, C., Valdez, B., Ayala, R., & Pérez, A. (2017). Quality assessment of biodiesel blends proposed by the new Mexican policy framework. *Energies*, *10*(5), 631; https://doi.org/10.3390/en10050631

Daud, S., Hamidi, M. A., & Mamat, R. (2022). A review of fuel additives' effects and predictions on internal combustion engine performance and emissions. In *AIMS Energy,* 10(1), 1-22; https://doi.org/10.3934/ENERGY.2022001

Debbarma, S., Misra, R. D., & Das, B. (2020). Performance of graphene-added palm biodiesel in a diesel engine. *Clean Technologies and Environmental Policy*, *22*(2), 523–534. https://doi.org/10.1007/s10098-019-01800-2

Deng, S., & Berry, V. (2016). Wrinkled , rippled and crumpled graphene : an overview of formation mechanism , electronic properties , and applications. *Biochemical Pharmacology*, *19*(4), 197–212. https://doi.org/10.1016/j.mattod.2015.10.002

Devarajan, Y., Munuswamy, D. B., & Mahalingam, A. (2018). Influence of nano-additive on performance and emission characteristics of a diesel engine running on neat neem oil biodiesel. In *Environmental Science and Pollution Research* 25(26), 26167-72; https://doi.org/10.1007/s11356-018-2618-6

EL-Seesy, A. I., & Hassan, H. (2019). Combustion characteristics of a diesel engine fueled by biodiesel-diesel-n-butanol blend and titanium oxide additives. *Energy Procedia*, *162* (April), 48–56. https://doi.org/10.1016/j.egypro.2019.04.006

El-Seesy, A. I., Hassan, H., & Ookawara, S. (2018). Effects of graphene nanoplatelet addition to jatropha Biodiesel–Diesel mixture on the performance and emission characteristics of a diesel engine. *Energy*, *147 (March)*, 1129–1152; https://doi.org/10.1016/j.energy.2018.01.108

Fazal, M. A., Haseeb, A. S. M. A., & Masjuki, H. H. (2013). Investigation of friction and wear characteristics of palm biodiesel. In *Energy Conversion and Management* 67(March), 251-256; https://doi.org/10.1016/j.enconman.2012.12.002

Gad, M. S., El-Araby, R., Abed, K. A., El-Ibiari, N. N., El Morsi, A. K., & El-Diwani, G. I. (2018). Performance and emissions characteristics of C.I. engine fueled with palm oil/palm oil methyl ester blended with diesel fuel. *Egyptian Journal of*

Petroleum, *27*(2), 215–219. https://doi.org/10.1016/j.ejpe.2017.05.009

Goswami, L., Kim, K. H., Deep, A., Das, P., Bhattacharya, S. S., Kumar, S., & Adelodun, A. A. (2017). Engineered nano particles: Nature, behavior, and effect on the environment. In *Journal of Environmental Management*, 196(July), 297-315; https://doi.org/10.1016/j.jenvman.2017.01.011

Hanaki, K., & Portugal-Pereira, J. (2018). *The Effect of Biofuel Production on Greenhouse Gas Emission Reductions*. Biofuels and sustainability (53-71); https://doi.org/10.1007/978-4-431-54895-9_6

Ivanov, I. (2019). Window To the Future. *Current Digest of the Russian Press, The*, *71*(048), 17–18. https://doi.org/10.21557/dsp.56774463

Jalaludin, H. A., Abdullah, N. R., Sharudin, H., Asiah, A. R., & Jumali, M. F. (2020). Emission characteristics of biodiesel ratios of 10%, 20%, and, 30% in a single-cylinder diesel engine. *IOP Conference Series: Materials Science and Engineering*, *834*(1). https://doi.org/10.1088/1757-899X/834/1/012066

Jeyaseelan, T., & Chako, N. (2020). Comparative evaluation of graphene oxide and graphene nanoplatelets as fuel additives on the combustion and emission characteristics of a diesel engine fuelled with diesel and biodiesel blend. *Fuel Processing Technology*, *204*(January), 106406. https://doi.org/10.1016/j.fuproc.2020.106406

Kamel, S., El-Sakhawy, M., Anis, B., & Tohamy, H. A. S. (2019). Graphene's Structure, Synthesis and Characterization; A brief review. *Egyptian Journal of Chemistry*, *62*(Part 2), 593–608. https://doi.org/10.21608/ejchem.2019.15173.1919

Mahdi, J. M., & Nsofor, E. C. (2017). Melting enhancement in triplex-tube latent heat energy storage system using nanoparticles-metal foam combination. In *Applied Energy,* 191(April), 22-34; https://doi.org/10.1016/j.apenergy.2016.11.036

Mallikarjuna Rao, D., Janga, V. S. R., Dhana Raju, V., & Arifa, S. (2022). Impact of Graphene Nanoparticles Addition to Jatropha Biodiesel Blend on the Performance and Emission Characteristics of a Diesel Engine. *Lecture Notes in Mechanical Engineering* design and energy technologies, (October), 825–33; https://doi.org/10.1007/978-981-16-4222-7_90

Masera, K., & Hossain, A. K. (2017). Production, Characterisation and Assessment of Biomixture Fuels for Compression Ignition Engine Application. *International Journal of Mechanical and Mechatronics Engineering*, *11*(12), 1857–1863. https://doi.org/10.1999/1307-6892/10008317

Nair, J., Prasad Kumar, P., Thakur, A. K., Samhita, & Aravinda. (2021). Influence on emissions and performance of CI engine with graphene nanoparticles blended with Karanja biodiesel. *AIP Conference Proceedings*, *2317*(February). https://doi.org/10.1063/5.0036142

Nandiyanto, A. B. D., Oktiani, R., & Ragadhita, R. (2019). How to read and interpret ftir spectroscope of organic material. *Indonesian Journal of Science and Technology*, *4*(1), 97–118. https://doi.org/10.17509/ijost.v4i1.15806

Osawa, W. O., Onyari, J. M., Sahoo, P. K., & Mulaa, F. J. (2014). Process optimization for production of biodiesel from croton oil using two-stage process. *IOSR Journal of Environmental Science, Toxicology and Food Technology*, *8*(11), 49–54. https://doi.org/10.9790/2402-081134954

Oseni, M., & Obetta, S. (2012). Evaluation of fatty acids profile of ethyl esters of yellow oleander and groundnut oils as biodiesel feedstock. *American Journal of Scientific and Industrial Research*, *3*(2), 62–68. https://doi.org/10.5251/ajsir.2012.3.2.62.68

Pattanaik, B. P., Jena, J., & Misra, R. D. (2017). The effect of oxygen content in soapnut biodiesel-diesel blends on performance of a diesel engine. *International Journal of Automotive and Mechanical Engineering*, *14*(3), 4574–4588. https://doi.org/10.15282/ijame.14.3.2017.14.0361

Pham, P. X. (2015). *Influences of Molecular Profiles of Biodiesels on Atomization, Combustion and Emission Characteristics*. PhD. thesis. University of Sydney; https://doi.org/10.13140/2.1.4430.1609

Qasim, M., Ansari, T. M., & Hussain, M. (2017). Combustion, performance, and emission evaluation of a diesel engine with biodiesel like fuel blends derived from a mixture of Pakistani waste canola and waste transformer oils. *Energies 10*(7), 1023; https://doi.org/10.3390/en10071023

Razzaq, L., Mujtaba, M. A., Elahi, M., Soudagar, M., Ahmed, W., Fayaz, H., Bashir, S., Fattah, I. M. R., Chyuan, H., Shahapurkar, K., Afzal, A., Wageh, S., Al-ghamdi, A., Shujaat, M., & El-seesy, A. I. (2021). Engine performance and emission characteristics of palm biodiesel blends with graphene oxide nanoplatelets and dimethyl carbonate additives. *Journal of Environmental Management*, *282*(October 2020), 111917. https://doi.org/10.1016/j.jenvman.2020.111917

Ruhul, A. M., Kalam, M. A., Masjuki, H. H., Fattah, I. M. R., Reham, S. S., & Rashed, M. M. (2015). State of the art of biodiesel production processes: A review of the heterogeneous catalyst. *RSC Advances*, *5*(122), 101023–101044. https://doi.org/10.1039/c5ra09862a

Sabapathy, S. P., Ammasi, A. M., Khalife, E., Kaveh, M., Szymanek, M., Reghu, G. K., & Sabapathy, P. (2021). Comprehensive assessment from optimum biodiesel yield to combustion characteristics of light duty diesel engine fueled with palm kernel oil biodiesel and fuel additives. *Materials*, 14(15), 4274; https://doi.org/10.3390/ma14154274

Sang, M., Shin, J., Kim, K., & Yu, K. J. (2019). Electronic and thermal properties of graphene and recent advances in graphene based electronics applications. In *Nanomaterials,* 9(3) 374; https://doi.org/10.3390/nano9030374

Saxena, V., Kumar, N., & Saxena, V. K. (2017). A comprehensive review on combustion and stability aspects of metal nanoparticles and its additive effect on diesel and biodiesel fuelled C.I. engine. In *Renewable and Sustainable Energy Reviews,* 70(April), 563–588); https://doi.org/10.1016/j.rser.2016.11.067

Semakula, M., & Inambao, P. F. (2018). The Formation, Effects and Control of Oxides of Nitrogen in Diesel Engines. *International Journal of Applied Engineering Research*, *13*(6), 3200–3209. https://www.ripublication.com/ijaer18/ijaerv13n6_09.pdf

SiSim, H. S., Yetter, R. A., Connell, T. L., Dabbs, D. M., & Aksay, I. A. (2020). (2020). Multifunctional Graphene-Based Additives for Enhanced Combustion of Cracked Hydrocarbon Fuels under Supercritical Conditions. *Combustion Science and Technology*, *192*(7), 1420–1435. https://doi.org/10.1080/00102202.2020.1737033

Sivasankaran, S., Sivaprasad, K., Narayanasamy, R., & Satyanarayana, P. V. (2011). X-ray peak broadening analysis of AA 6061100−x−xwt.% Al2O3 nanocomposite prepared by mechanical alloying. *Materials Characterization*, *62*(7), 661–672. https://doi.org/10.1016/j.matchar.2011.04.017

Soudagar, M. E. M., Nik-Ghazali, N.-N., Abul Kalam, M., Badruddin, I. A., Banapurmath, N. R., & Akram, N. (2018). The effect of nano-additives in diesel-biodiesel fuel blends: A comprehensive review on stability, engine performance and emission characteristics. *Energy Conversion and Management*, *178*, 146–177. https://doi.org/10.1016/j.enconman.2018.10.019

Soudagar, M. E. M., Nik-Ghazali, N.-N., Kalam, M. A., Badruddin, I. A., Banapurmath, N. R., Bin Ali, M. A., Kamangar, S., Cho, H. M., & Akram, N. (2020). An investigation on the influence of aluminium oxide nano-additive and honge oil methyl ester on engine performance, combustion and emission characteristics. *Renewable Energy*, *146*, 2291–2307. https://doi.org/10.1016/j.renene.2019.08.025

Sunilkumar, T., Manavendra, G., Banapurmath, N.R., Guruchethan, A.M. (2017). Performance and Emission Characteristics of Graphene Nano Particle-Biodiesel Blends Fuelled Diesel Engine. *International Research Journal of Engineering and Technology (IRJET)*, *4*(10), 552-557. https://www.irjet.net/archives/V4/i10/IRJET-V4I1096.pdf

Pallone, T. (2018). 13 Reasons Graphene Is a "Wonder Material." In https://www.globalspec.com

Ujjain, S. K., Bhatia, R., & Ahuja, P. (2019). Aziridine-functionalized graphene: Effect of aromaticity for aryl functional groups on enhanced power conversion efficiency of organic photovoltaic cells. In *Journal of Saudi Chemical Society,* 23(6), 655–665; https://doi.org/10.1016/j.jscs.2018.11.006

Wade, Jr., L. G. (2003). *IR*: *Theory and Interpretation of IR spectra presentation*, *5th edn*, *Organic Chemistry*, 853–866.

Yarkasuwa, C. I., Wilson, D., & Michael, E. (2013). Production of biodiesel from yellow oleander (thevetia peruvian) oil and its biodegradability. *Journal of the Korean Chemical Society*, *57*(3), 377–381. https://doi.org/10.5012/jkcs.2013.57.3.377

Yohannan Panicker, C., Varghese, H. T., & Chandran, A. (2011).

Densityfunctional theory and IR spectroscopic study of carboxyl group. *Oriental Journal of Chemistry*, *27*(4), 1771–1774. https://www.orientjchem.org/?p=24331